Check for updates

Phosphate adsorption onto thermally dehydrated aluminate cement granules

Zhenglin Zha, [ID] [a] Yongxiang Ren,*[a] Shaobin Wang, [ID] *[b] Zhuang Qian,[a] Lei Yang,[a] Peng Cheng,[a] Yun Han[a] and Man Wang[c]

Phosphorus is the main element for eutrophication of water bodies. Aluminate cement is a cheap building material rich in aluminium and calcium which have significant effects on phosphate adsorption. This study aimed at the investigation of removal behavior of phosphate by thermally dehydrated aluminate cement granules, treated at different temperatures, and the adsorption mechanisms. It was found that 600 °C was the optimal temperature, producing excellent granules with a particle size of 0.6–1.5 mm (T600), giving a great adsorption capacity of phosphate of 49.1 mg P per g and presenting fast and high initial adsorption, reaching a capacity of 23.7 mg P per g within 30 min at 20 °C. The phosphate adsorption process was dominated by chemical adsorption, mainly through inner-sphere complexion and phosphate precipitation on the surface of the adsorbent. Compared with other phosphate adsorbents, T600 may be an economical and efficient adsorbent.

1 Introduction

Eutrophication has become a worldwide problem as a large number of nutrients are discharged into water bodies. Eutrophication can cause the degradation of ecological environment of water bodies, and blooms of red tide and blue-green algae, which cause the death of aquatic animals and many other environmental issues.[1,2] Phosphorus is believed to be one of the main reasons for the eutrophication of water bodies. It is the limiting element of eutrophication and the nutrient presented in the lowest amount associated with phytoplankton requirements.[3–5] Phosphorus emission from increased use of fertilizers into water causes about 30–50% of the eutrophication problem.[6] Therefore, removal of phosphorus from water is important for controlling the eutrophication of water bodies.[7]

There are various techniques for the removal of phosphorus, such as biological removal, chemical precipitation and adsorption.[8,9] Among them, adsorption has attracted more and more attention due to its efficiency, simple operation and lack of secondary pollution compared to other methods. However, it suffers from some demerits, such as low removal capacity and high cost of adsorbents.[10–12]

In the past few years, great progress has been made in the development of high-capacity and low-cost adsorbents for phosphate adsorption. Previous research showed that aluminium, iron and calcium in a material have a positive effect on phosphate adsorption, and the materials rich in aluminium and calcium showed better adsorption capacities, such as hydrated Portland cement,[13] activated aluminium oxide[14] and red mud.[15]

Aluminate cement is a cementations material, mainly composed of calcium aluminate with 50% of alumina content, and thus has a great potential for adsorption of phosphorus. Aluminate cement has been produced in large quantities in China, being an economical and efficient phosphorus adsorbent. However, its adsorption behaviour in phosphate removal has not been well investigated. In this paper, the use of aluminate cement as an adsorbent for phosphate removal from wastewater was reported and the adsorption characteristics and mechanism were revealed.

2 Material and methods

2.1 Preparation of adsorbents

A commercially available aluminate cement (grade CA50-A700, Zhengzhou, China) was used to prepare hydrated aluminate cement granules (HAC), and the bulk chemical compositions

[a]*Key Laboratory of Northwestern Water Resource and Environment Ecology of Ministry of Education, Shaanxi Key Laboratory of Environmental Engineering, Xi'an University of Architecture and Technology, Xi'an 710055, China. E-mail: ryx@xauat.edu.cn*
[b]*Department of Chemical Engineering, Curtin University, GPO Box U1987, Perth, Western Australia 6845, Australia. E-mail: shaobin.wang@exchange.curtin.edu.au*
[c]*Tianshui Soil and Water Conservation Scientific Experiment Station, The Yellow River Water Conservancy Commission, Tianshui 741000, Gansu, China*

Table 1 Bulk chemical analysis of the aluminate cement

Composition	Al_2O_3	CaO	Fe_2O_3	SiO_2	MgO	$(K, Na)_2O$
Mass fraction (%)	50.6	33.2	2.0	7.8	1.8	0.3

are shown in Table 1. A slurry was firstly prepared by mixing distilled water with 500 g of aluminate cement at a water-cement ratio of 0.45. The slurry was kept sprinkling regularly for 3 days for hardening and 2 days for paste drying at room temperature. After the curing, the solid was crushed and then sieved to a particle size of 0.6–1.5 mm. The thermally dehydrated aluminate cement granules (THACs) were prepared by thermal activation at a temperature range of 100–900 °C for 2 h. The samples were named as HT, where T is the temperature.

2.2 Characterization of adsorbents

The specific surface area of the samples was determined by N_2 adsorption–desorption isotherms on a V-Sorb2800P at liquid N_2 temperature (Gold APP Instrument Corporation, China). Thermogravimetric analysis (TGA/DSC1/1600, Switzerland) was used to determine the weight loss at a heating rate of 10 °C min^{-1}. The morphology and zeta potentials of adsorbents before and after phosphate adsorption were determined by a Quanta 650 FEG scanning electron microscope (SEM, FEI Corporation, USA) and a zeta potential instrument (Malvern Instruments Ltd., UK), respectively. X-ray diffraction (XRD) was used to identify the mineral phases on a DMAX—2400X diffractometer (Rigaku Corporation, Japan) with CuKα radiation (44 kV, 100 mA) and Ni filter, from 10–80° at a scan speed of 4° min^{-1}. Fourier transform infrared spectroscopy (FTIR, IRPrestige-21, Shimadzu Corporation, Japan) was applied to verify the functional groups in the 500–4000 cm^{-1} spectral range.

The strength of adsorbents is represented by the loss rate of mass (Lorm). The Lorm was tested by mixing 5 g of the adsorbents into 50 mL distilled water and stirred at 160 rpm in a shaker for 12 h. Then the adsorbents were taken out, dried and weighed. The Lorm was calculated according to eqn (1):

$$\text{Lorm} = \frac{m - m_1}{m} \times 100\% \tag{1}$$

where m and m_1 are the initial and final weights of the adsorbents (g), respectively.

2.3 Phosphate adsorption experiments

Phosphate solutions were prepared by dissolving a certain amount of pure KH_2PO_4 in distilled water. All the phosphate adsorption experiments were carried out in 250 mL conical glass flasks with a fixed dose of adsorbents at 2 g L^{-1}.

Typically, the adsorbent of 0.4 g was mixed into a 200 mL phosphate solution with the initial P concentration of 100 mg L^{-1}. The solutions were agitated at 160 rpm in a thermostatic shaker at temperature of 20 °C for 48 h. The phosphate adsorption capacity (q) was calculated from eqn (2).

$$q = \frac{C_0 - C_1}{m} \times V \tag{2}$$

where C_0, C_1 are the initial and residual P concentrations (mg L^{-1}), respectively; V is the volume of the solution (L); and m is the mass of adsorbents (g).

The phosphate adsorption kinetics was studied in batch experiments at an initial P concentration of 100 mg L^{-1} and temperatures of 4 and 20 °C. The residual phosphate in solution was measured at predetermined intervals, and the equilibrium time was obtained when the residual P concentrations remain constantly.

The adsorption isotherm experiments were carried out for 48 h at 4 and 20 °C with the initial P concentration ranged from 100 to 3000 mg L^{-1}. For the study on the influence of initial solution pH, the pH of solution was adjusted from 3 to 11 with 0.1 mol L^{-1} NaOH or HCl solutions before adding the adsorbent. The initial P concentration was 100 mg L^{-1}, the contact time was 48 h and the temperature was 20 °C. The effect of various anions on the phosphate adsorption behaviour was also examined at the conditions, the initial P concentration of 100 mg L^{-1}, the concentrations of CO_3^{2-}, SO_4^{2-}, and NO_3^- in the form of their sodium salts at 3, 6 and 15 mmol L^{-1}, equilibrium time of 48 h and temperature of 20 °C. The effect of ionic strength on phosphate adsorption was tested in NaCl solutions at concentrations of 0.005–0.5 mol L^{-1}.

3 Results and discussion

3.1 Effect of thermal activation temperature

The specific surface area and pore volume of adsorbent materials have an important influence on the adsorption capacity. The specific surface area (S, m^2 g^{-1}) and pore volumes (V, m^3 g^{-1}) of the prepared materials are illustrated in Table 2. Generally, the surface area and pore volume increase with the

Table 2 The specific surface area, pore volume, loss rate of mass and phosphate adsorption capacities of HAC and THACs

Sample	BET surface area (S) (m^2 g^{-1})	Pore volume (V) (cm^3 g^{-1})	Loss rate of mass (Lorm) (%)	Adsorption capacities (mg P per g)
HAC	5.4	0.14	4.2	16.2
T100	7.0	0.14	5.6	18.8
T200	17.6	0.15	10.6	24.6
T300	19.6	0.19	11.7	34.7
T400	19.9	0.21	6.9	22.7
T500	20.1	0.14	6.4	25.8
T600	24.0	0.24	6.6	49.1
T700	24.8	0.21	11.4	50.1
T800	11.7	0.16	19.6	36.0
T900	7.2	0.12	34.6	34.6

increased temperature and reach the maximum at 600–700 °C. At activation temperatures of 600 and 700 °C, the V values are 0.21 cm³ g⁻¹ and 0.24 cm³ g⁻¹, respectively. The S values of samples T600 and T700 are 24.0 and 24.8 m² g⁻¹, respectively, which are about 5 times as high as that of HAC. The S and V decrease sharply at 900 °C, giving 7.2 m² g⁻¹ and 0.12 cm³ g⁻¹, respectively. The results indicated that thermal treatment could increase the S and V of HAC.

Loss rate of mass (Lorm) of HAC and THACs are summarized in Table 2. The Lorm increased with the increasing temperature up to 300 °C; the Lorm changed little at 400–600 °C. Then the Lorm increased rapidly at the activation temperature higher than 600 °C. The Lorm of T900 reached 34.6%, which was about more than 6 times as high as that of T600.

TGA curve of HAC is shown in Fig. 1. It can be observed that the weight of HAC sharply decreased by 21.2% between the ambient temperature to 300 °C. The weight loss of HAC decreased at about 2.9% between 300 °C to 400 °C and then 3.6% from 400 °C to 1000 °C. The HAC is mainly composed of $2CaO \cdot Al_2O_3 \cdot 8H_2O$ (C_2AH_8) and $Al(OH)_3$.[16,17] At a temperature below 300 °C, the HAC is very sensitive to the temperature, and free water is lost by evaporation as well as C_2AH_8 converted to $3CaO \cdot Al_2O_3 \cdot 6H_2O$ (C_3AH_6), leading to the increase of porosity and the decline of structural stability.[18,19] After exposure to 400–600 °C, slowly excessive dehydration of C_3AH_6 and $Al(OH)_3$ occurred, leading to the formation of $12CaO \cdot 7Al_2O_3$ ($C_{12}A_7$).[18,20] Previous reports showed that the decomposition of limestone and the collapse of the structure happened till 800–900 °C, inducing a rapid decline in the porosity and the structural stability.[19,21] These may be the reasons for the least Lorm at 400–600 °C.

Table 2 also shows the phosphate adsorption capacities of HAC and THACs. Thermally treated THACs had different adsorption capacities of phosphate. The adsorption capacity of HAC is only 16.2 mg g⁻¹. With the increase of temperature, the adsorption capacity of THACs fluctuated. The adsorption capacities of phosphate on T600 and T700 were 49.1 and 50.1 mg g⁻¹, respectively, which are 3 times higher than that of HAC for phosphate adsorption. This may be attributed to the larger BET

surface area and pore volume of T600 and T700. However, the adsorption capacity of T900 dropped to 33.6 mg g⁻¹.

As it is seen, T600 and T700 had the similar adsorption capacity while the Lorm of T600 was far less than that of T700. Therefore, T600 was selected as a better adsorbent for further research.

3.2 Adsorption kinetics

Fig. 2 presents dynamic adsorption of phosphate on T600 at 4 and 20 °C. The adsorption was initially fast and reached the equilibrium in 48 h. In addition, higher temperature significantly improved adsorption capacity. Both the pseudo-first-order (PFO) and pseudo-second-order (PSO) kinetic models were used for modelling the sorption kinetics. The PFO kinetic model could be expressed in eqn (3):

$$q_t = q_e(1 - e^{-k_1 t}) \tag{3}$$

The PSO kinetic model was represented by eqn (4):

$$q_t = k_2 q_e^2 t / (1 + k_2 q_e t) \tag{4}$$

where q_e and q_t are the amounts (mg L⁻¹) of phosphate adsorbed at equilibrium and time t, respectively. The k_1 (h⁻¹) and k_2 (g (mg⁻¹ h⁻¹)) represented the rate constants of PFO and PSO adsorption kinetic models, respectively.

The fitting curves by the PFO and PSO kinetic models are demonstrated in Fig. 2. Table 3 lists the kinetic parameters and the correlation coefficients (R^2). The R^2 for the PSO kinetic model was higher than that for the PFO kinetic model, and the q_e values calculated by the PSO kinetic model were much closer to the experimental q_e values, verifying that the adsorption process could be better described by the PSO kinetic model. These indicated that the adsorption of phosphate onto T600 might a chemical adsorption dominated process.[22–24] Moreover, the phosphate desorption in water was 1.7 mg g⁻¹, only 3.5% of
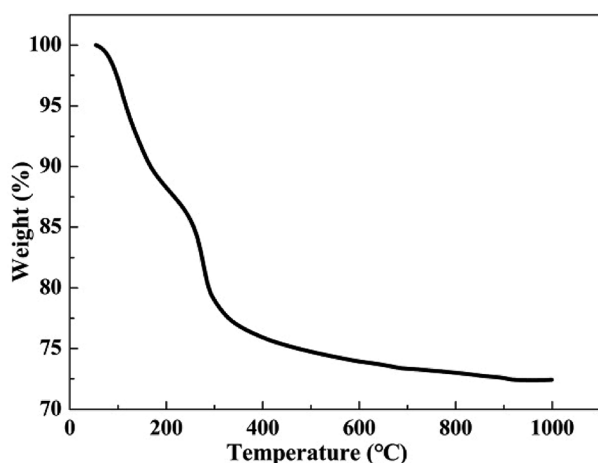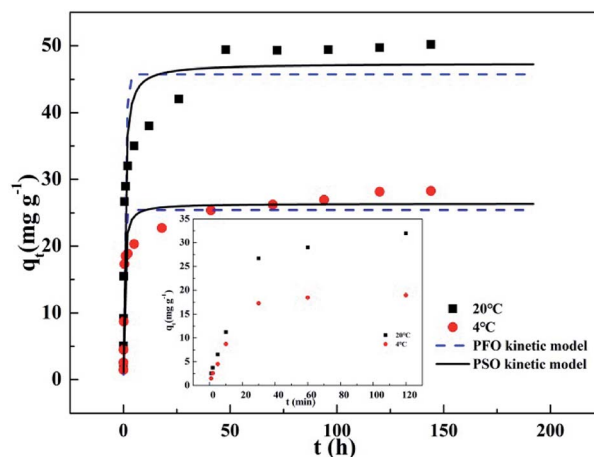

Fig. 1 TGA curve of HAC.

Fig. 2 Adsorption kinetics of phosphate removal on T600 at 4 and 20 °C.

Table 3 Fitting parameters of the PFO and PSO adsorption kinetic models

T (°C)	The PFO kinetic model			The PSO kinetic model		
	$q_{e.cal}$ (mg g^{-1})	k_1 (h^{-1})	R^2	$q_{e.cal}$ (mg g^{-1})	k_2 (g (mg^{-1} h^{-1}))	R^2
4	25.4	1.84	0.906	26.4	0.10	0.953
20	45.8	1.18	0.885	47.3	0.040	0.943

Table 4 The adsorption capacities of phosphate on T600 and reported adsorbents

Adsorbents	Adsorption capacity (mg P per g)	Initial P concentration (mg P per L)	Initial pH	Dosage (g L^{-1})	Equilibrium time (h)	Morphology
Synthesized Zn–Al LDH[25]	46.5	310	7	5	4	Powder
Hydroxyl-aluminium pillared bentonite[29]	11.2	60	3	4	6	Powder
Zero valent iron[26]	35.5	200	7.2 ± 0.2	2.5	4	Powder
ZrO$_2$ nanoparticle[22]	99.0	50	6.2	0.5	8	Powder
Lanthanum oxide[14]	40	100	5	2.5	24	Particle (1.18 mm)
Magnetic Fe–Zr oxide nanoparticle[30]	16.6	50	4 ± 0.2	2	24	Powder
Activated aluminium oxide[14]	20	50	5	2.5	24	Particle (1.18 mm)
Fe–Mn oxide[12]	11	40	7.0	2.5	5	Particle (1–3 mm)
Ca(OH)$_2$ treated clinoptilolite[27]	6	100	7	10	168	Particle (1.2–2 mm)
Thermally treated red mud[28]	8.4	50	6.0	4	6	Particle (1.5 mm)
T600	49.1	100	4.8 ± 0.1	2	48	Particle (0.6–1.5 mm)

adsorbed phosphate, also demonstrating strong chemical bonding and a chemical adsorption dominated process.

Table 4 summarizes the adsorption capacities of some adsorbent materials in phosphate removal in literature. T600 exhibited a great adsorption capacity. Some adsorbents, such as synthesized Zn–Al LDH,[25] zero valent iron,[26] ZrO$_2$ nanoparticle[22] and lanthanum oxide,[14] showed a large adsorption capacity. However, they were fine powders and there will be a lot of problems in practical engineering applications, such as difficult for separation and easily lost in operation. Moreover, the rare-earth metal Zr and La based materials are expensive. Meanwhile, the adsorption capacities of other cheaper materials, activated aluminium oxide,[14] Fe–Mn oxide,[12] Ca(OH)$_2$ treated clinoptilolite[27] and thermally treated red mud,[28] were significantly less than T600. On the contrary, T600 has a wide source, low price and large particle size. Although its equilibrium period was relatively longer (Fig. 2), T600 presents fast and high initial adsorption, reaching a capacity of 23.7 mg g^{-1} within 30 min at 20 °C, which was 50% of the total adsorption capacity.

3.3 Adsorption isotherms

The relationship between amount of adsorbed phosphate onto T600 and its equilibrium concentration was established with both Langmuir and Freundlich isotherm models as given in eqn (5) and (6), respectively:

$$q_e = q_m K_L C_e / (1 + K_L C_e) \qquad (5)$$

$$q_e = K_F C_e^{\frac{1}{n}} \qquad (6)$$

where q_e is the adsorption amount (mg g^{-1}) of phosphate at equilibrium, q_m is the Langmuir saturated adsorption capacity (mg g^{-1}), K_L is the Langmuir equilibrium constant, K_F and n are the Freundlich constants, $1/n$ is an empirical parameter relating the adsorption intensity, which varies with the heterogeneity of the materials. The adsorption isotherms and models for phosphate by T600 are shown in Fig. 3 and the fitting parameters of the Langmuir and Freundlich isotherm models are listed in Table 5.

The low R^2 (0.800 and 0.744) value from the Langmuir isotherm indicates that the model is not well suited to describe the adsorption of phosphate by T600. The R^2 value (0.956 and
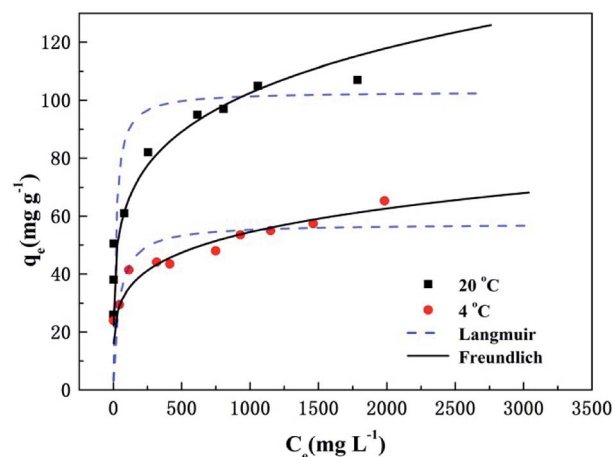

Fig. 3 Adsorption isotherms and models of phosphate removal on T600.

Table 5 Fitting parameters of Langmuir and Freundlich adsorption isotherm model

T (°C)	Langmuir isotherm model			Freundlich isotherm model		
	q_m (mg g^{-1})	K_L (L mg^{-1})	R^2	K_F	$1/n$	R^2
4	57.44	0.03	0.800	13.52	0.20	0.956
20	102.98	0.06	0.744	25.39	0.20	0.970

0.970) for the Freundlich isotherm is relatively higher than that of the Langmuir isotherm. Thus, these results suggest that the adsorption of phosphate onto T600 can be best described by the Freundlich isotherm model, which assumes multilayer adsorption on heterogeneous surfaces.[31] In addition, the values of $1/n$ at two temperatures are less than one, indicating that the process of phosphate adsorption on T600 is favourable.[25,32]

3.4 Effect of pH

The influence of initial pH on the phosphate adsorption capacity of T600 is demonstrated in Fig. 4. The solution pH has an important impact on the adsorption process. With the increased pH, the adsorption capacity decreased significantly, which was probably due to the changes in surface charge of T600 and phosphate species.

The low pH of solution is beneficial to the surface protonation of adsorbents, and the adsorption properties can be improved by the enhanced electrostatic attraction between phosphate anions and the surface of T600.[22] With the increase of pH, the positive charge on the surface of the adsorbent reduced. Hence, fewer amounts of the negatively charged phosphate ions will be attracted to the surface of the adsorbent, which may cause a decreased phosphate adsorption capacity. Besides, according to the dissociation equilibrium of phosphate in aqueous solution ($H_3PO_4 \rightleftharpoons H^+ + H_2PO_4^-$, p$K_{a1} = 2.12$; $H_2PO_4^- \rightleftharpoons H^+ + HPO_4^{2-}$, p$K_{a2} = 7.21$; $HPO_4^{2-} \rightleftharpoons H^+ + PO_4^{3-}$, p$K_{a3} = 12.33$), HPO_4^{2-} and $H_2PO_4^-$ were the major species of

phosphate at pH 3–11, which were negatively charged.[33] Phosphate adsorption decreased with the increase of pH due to the enlargement amount of HPO_4^{2-}. The competitive effect of OH^- and phosphate anions on the adsorption sites at high pH also caused the reduction of phosphate adsorption capacity.[34] Moreover, the speciation of cations may be another reason, and aluminium forms cationic species at lower pH (such as Al–OH_2^+), which are easy to react with phosphate ions. However, at higher pH, a part of aluminium forms neutral species (such as Al–OH) and anionic species (such as AlO_2^- or $Al(OH)_4^-$), making them harder to react with phosphate.[14,35] Hence, the phosphate adsorption on T600 was better under neutral and acidic conditions.

3.5 Effect of coexisting anions

The compositions of natural aquatic ecosystems and actual wastewater are complex and contain many other anions, which might compete with phosphate for the adsorption on T600. Therefore, the effects of several anions (CO_3^{2-}, SO_4^{2-} and NO_3^-) on phosphate adsorption on T600 were examined (Fig. 5). The concentration of phosphate was 100 mg P per L (3.23 mmol L^{-1}) and coexisting anions concentrations were varying at 3, 6 and 15 mmol L^{-1}.

NO_3^- had little effect on phosphate adsorption, suggesting no significant influence by monovalent anions. However, SO_4^{2-} and CO_3^{2-} had a great negative effect on phosphate adsorption, reflecting that polyvalent anions were easier to be adsorbed than monovalent anions.[36] The effect of SO_4^{2-} concentration at 3–15 mmol L^{-1} on phosphate adsorption remained the same while CO_3^{2-} concentration generated a remarkable influence on phosphate adsorption. The adsorption capacity of phosphate decreased by 90% at CO_3^{2-} concentration of 15 mmol L^{-1}.

It has been reported that CO_3^{2-} had strong competition for the adsorption sites on the adsorbent with phosphate ions.[30] Moreover, the pH value of solution significantly increased with the addition of CO_3^{2-} [36] and the initial pH of solution was 10.7 at the concentration of 15 mmol L^{-1}, which would cause a sharp decrease of phosphate adsorption capacity, as shown in Fig. 5.
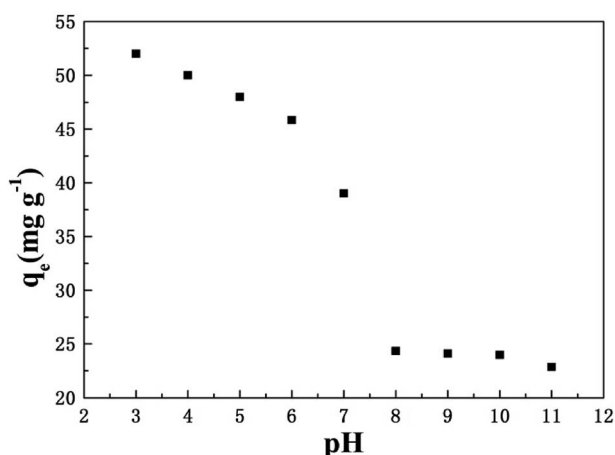
Fig. 4 Effect of initial pH on phosphate adsorption by T600.
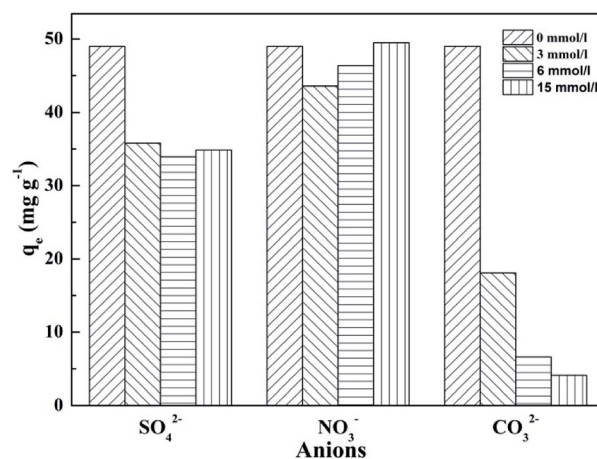
Fig. 5 Effect of coexisting anions on phosphate adsorption by T600.

Thus, the result showed that T600 had a good selectivity for phosphate adsorption to monovalent anions, but polyvalent anions had a significantly negative influence on the adsorption, in particular, CO_3^{2-}.

3.6 Discussion on phosphate adsorption mechanisms

3.6.1 Adsorption thermodynamics. The thermodynamic parameters, free energy (ΔG), standard enthalpy (ΔH) and standard entropy (ΔS), can be determined by the following equations.

$$\Delta G = -RT \ln K_D \tag{7}$$

$$\Delta G = \Delta H - T\Delta S \tag{8}$$

$$\ln K_D = -\left(\frac{\Delta H}{R}\right)\left(\frac{1}{T}\right) + \frac{\Delta S}{R} \tag{9}$$

where R is universal gas constant (8.314 J (mol^{-1} K^{-1})) and T is temperature (K). K_D is the equilibrium constant of the distribution of phosphate between the solid and the liquid phases at equilibrium, and it was computed by the method of plotting $\ln(q_e/C_e)$ *versus* q_e by extrapolating q_e to zero.[37–39] The thermodynamic parameters for the adsorption of phosphate onto T600 were calculated and are summarized in Table 6.

The positive value of ΔH (42.7 kJ mol^{-1}) showed that phosphate adsorption on T600 was an endothermic reaction and chemisorption dominated process. The negative values of ΔG indicated that the phosphate adsorption process onto T600 was favourable and spontaneous.[38] Also, the value of ΔG decreased (-1.76 to -4.36 kJ mol^{-1}) with the increased temperature from 4 to 20 °C, which directly signified the enhanced feasibility of adsorption process at higher temperature. In addition, the positive value of ΔS indicated the increase in randomness during the adsorption process of phosphate ions on the active sites of T600.[40]

3.6.2 Effect of ionic strength. The effect of ionic strength on phosphate adsorption by T600 is shown in Fig. 6 and it demonstrates that the variations in the ionic strength of the phosphate solution has no remarkable effects on phosphate adsorption. Outer-sphere (nonspecific adsorption) and inner-sphere (specific adsorption) complex are two widely identifiable mechanisms for the adsorption of a solute onto a solid surface.[13,41] Outer-sphere complexation involves electrostatics attraction and it is strongly sensitive to ionic strength.[13,42] The adsorption of phosphate would decrease with the increase of ionic strength when it follows outer-sphere complex.[22] Inner-sphere complexation results in stronger adsorption than outer-sphere complexation and it shows little sensitivity to ionic
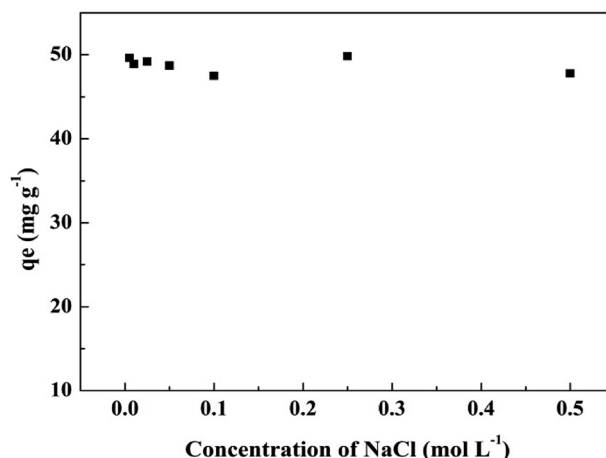

Fig. 6 Effect of ionic strength on phosphate adsorption by T600.

strength or a greater adsorption at higher ionic strength condition.[13,41,42] Thus, the adsorption of phosphate on to T600 follows the inner-sphere complex mechanism since the adsorption capacity was almost not affected by the ionic strength.

3.6.3 Zeta potential study. Zeta potential study has been used to verify outer-sphere or inner-sphere complexation of adsorbed ions on solid surface. The zeta potentials of T600 before and after phosphate adsorption are shown in Fig. 7. The Zeta potential of T600 decreased with increasing pH and it is apparent that T600 surface contains positive charge at pH below isoelectric point (IEP) and negative charge when pH is adjusted to higher than IEP. This phenomenon results in a decrease in the adsorption capacity of anions by T600 at higher pH. The adsorption of phosphate decreases the zeta potential of T600 at a given pH and shifts the IEP toward low pH values. The IEP of T600 before phosphate adsorption is 9.7 and it decreases to 7.9 after phosphate adsorption. The formation of inner-sphere complexes decreases the pH of IEP and the degree of reduction is related to solid surface, ions and their concentration, while the formation of outer-sphere complexes cannot change
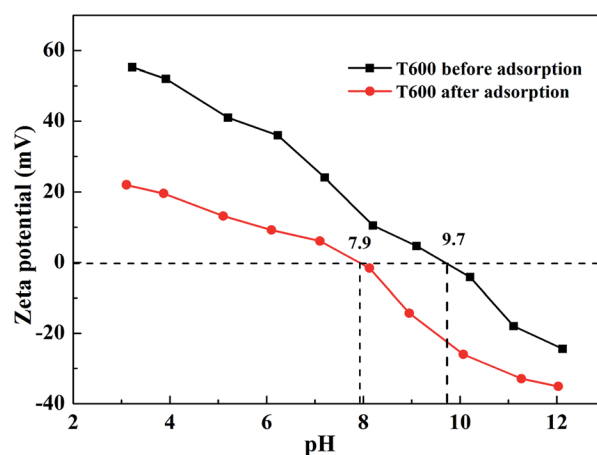
Table 6 Thermodynamic parameters for the adsorption of phosphate to the T600

T (°C)	ΔH (kJ mol^{-1})	ΔS (J mol^{-1})	ΔG (kJ mol^{-1})
20	42.7	154.1	-4.36
4			-1.76

Fig. 7 Zeta potential of T600 before and after phosphate adsorption.

the IEP of solids.[22,43,44] Therefore, the specific adsorption between T600 and phosphate is to form inner-sphere complexes on the T600.[22,43]

3.6.4 FTIR study. The Fourier transform infrared spectroscopy (FTIR) was used to identify the functional groups of T600 before and after phosphate adsorption (Fig. 8). The peaks at 3458 and 1640 cm^{-1} are originated from the strong hydroxyl stretching and bending vibrations of physically adsorbed H_2O or structural hydroxyl groups.[22] The peak at 802 cm^{-1} attributed to Al–O was extremely weakened after phosphate adsorption, which might be ascribed to the reason that a part of Al–O reacted with phosphate and then separated from T600, indicating that the Al–O played an important role in the adsorption process.[41,45] In addition, new peaks at 1010 and 510 cm^{-1} refer to the P=O bond, proving that phosphate ions were successfully adsorbed onto the adsorbent surface.

3.6.5 XRD study. X-ray diffraction (XRD) was used to further investigate phosphate adsorption (Fig. 9). The XRD pattern of T600 before adsorption shows the major peaks similar to those of T600 after adsorption, indicating that they have a similar composition, such as $Ca_2Al_2SiO_7$, $Ca_3Al_2O_6 \cdot 6H_2O$, and $CaAl_2O_4$, which were the components or hydration products of aluminate cement. However, two new peaks occurred at the range from 10° to 30°, which could be attributed to $Al(H_2PO_4)_3$ (PDF #14-0377) and $CaHPO_4$ (PDF #09-0077), illustrating that phosphate ion successfully adsorbed onto the adsorbent surface and phosphate precipitation occurred in the adsorption process.

3.6.6 SEM study. The surface morphologies of T600 before and after phosphate adsorption were analysed. SEM images showed rough surface of T600 (Fig. 10a) with irregular sheet structure (Fig. 10b). After phosphate adsorption, the surface morphology of T600 showed a significant difference (Fig. 10c). On one hand, the T600 surface became smooth due to the scour of water during the adsorption process; on the other hand, there were many flaky substances and small particles. Furthermore, it could be observed that the surface of T600 was covered with small spherical particles under high magnification (Fig. 10d), which would be the phosphate precipitates according to the
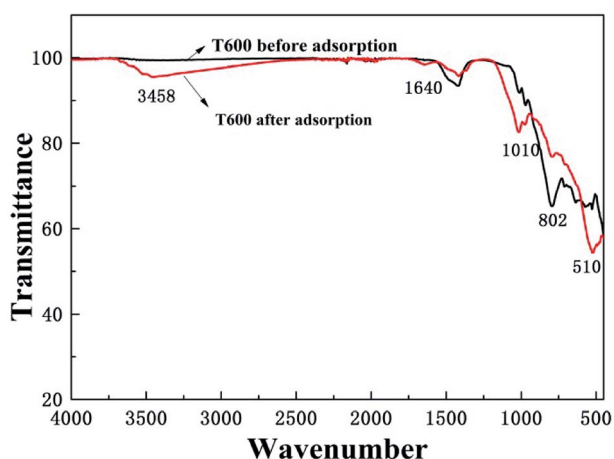

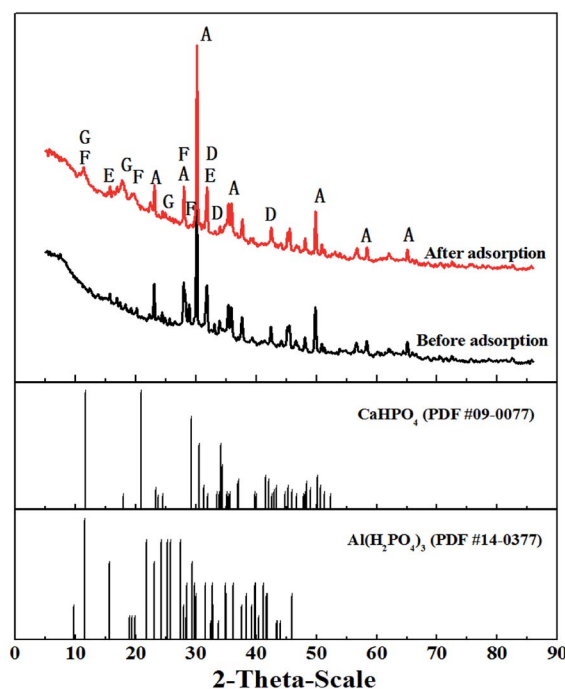Fig. 9 XRD patterns of T600 before and after phosphate adsorption (A – $Ca_2Al_2SiO_7$; D – $Ca_3Al_2O_6 \cdot 6H_2O$; E – $Ca_{12}Al_{14}O_{33}$; F – $CaHPO_4$; G – $Al(H_2PO_4)_3$).

FTIR and XRD studies. It is indicated that chemical adsorption occurred in the phosphate adsorption process. Although the large amount of the precipitates on the surface of T600 adsorbents would block the pores for against the second use of the adsorbents, it proved that phosphorus was effectively immobilized on the adsorbents, which might be a solution for the efficient recovery of phosphorus.
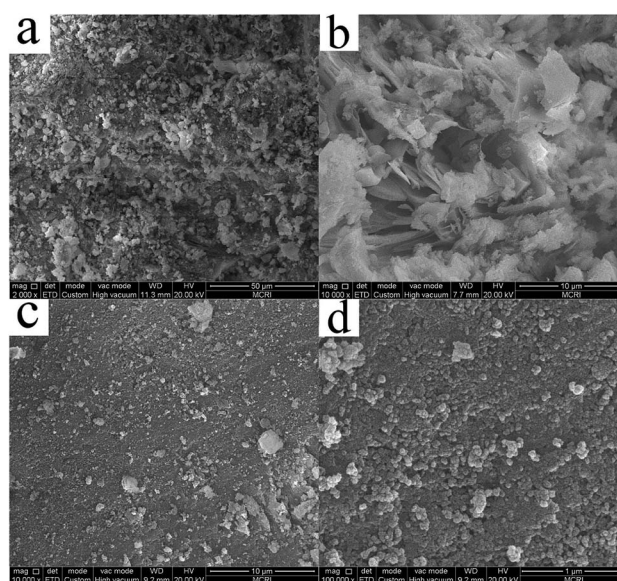

Fig. 10 SEM images of T600 before and after phosphate adsorption: (a) before adsorption ×2000; (b) before adsorption ×10 000; (c) after adsorption ×10 000; (d) after adsorption ×100 000.

Fig. 8 FTIR spectra of T600 before and after phosphate adsorption.

4   Conclusion

Thermal activation of hydrated aluminate cement was investigated for improved phosphate adsorption in aqueous solution. At the optimum activation temperature of 600 °C, sample T600 can reach 23.7 mg P per g rapidly in 30 min and equilibrium adsorption capacity of 49.1 mg P per g at 20 °C and pH of 4.8. Moreover, T600 has a good selectivity for phosphate adsorption to several coexisting ions. The adsorption of phosphate onto T600 was dominated by chemical adsorption, mainly through inner-sphere complexion and phosphate precipitation on the surface. T600 is an economical and efficient phosphate adsorbent for its low cost, large adsorption capacity and engineering practicability for addressing eutrophication problem.

Conflicts of interest

There are no conflicts to declare.

Acknowledgements

Notes and references

1 S. P. Boeykens, M. N. Piol, L. Samudio Legal, A. B. Saralegui and C. Vázquez, *J. Environ. Manage.*, 2017, **203**, 888–895.
2 P. M. Glibert, *Mar. Pollut. Bull.*, 2017, **124**, 591–606.
3 O. F. Schoumans, W. J. Chardon, M. E. Bechmann, C. Gascuel-Odoux, G. Hofman, B. Kronvang, G. H. Rubæk, B. Ulén and J. M. Dorioz, *Sci. Total Environ.*, 2014, **468–469**, 1255–1266.
4 J. Huang, C.-c. Xu, B. G. Ridoutt, X.-c. Wang and P.-a. Ren, *J. Cleaner Prod.*, 2017, **159**, 171–179.
5 J. Liu, G. Wang, L. Lu, Y. Guo and L. Yang, *RSC Adv.*, 2017, **7**, 40965–40972.
6 L. Fang, R. Liu, J. Li, C. Xu, L.-Z. Huang and D. Wang, *Water Res.*, 2018, **130**, 243–254.
7 R. P. Kralchevska, R. Prucek, J. Kolařík, J. Tuček, L. Machala, J. Filip, V. K. Sharma and R. Zbořil, *Water Res.*, 2016, **103**, 83–91.
8 L. Song, J. Huo, X. Wang, F. Yang, J. He and C. Li, *Chem. Eng. J.*, 2016, **284**, 182–193.
9 W. Wang, C. Ma, Y. Zhang, S. Yang, Y. Shao and X. Wang, *J. Environ. Sci.*, 2016, **45**, 191–199.
10 P. Zhang, T. Wang, G. Qian, D. Wu and R. L. Frost, *J. Colloid Interface Sci.*, 2014, **426**, 44–47.
11 X. Cui, X. Dai, K. Y. Khan, T. Li, X. Yang and Z. He, *Bioresour. Technol.*, 2016, **218**, 1123–1132.
12 X. Du, Q. Han, J. Li and H. Li, *J. Taiwan Inst. Chem. Eng.*, 2017, **76**, 167–175.
13 J. Y. Park, H. J. Byun, W. H. Choi and W. H. Kang, *Chemosphere*, 2008, **70**, 1429.
14 J. Xie, Y. Lin, C. Li, D. Wu and H. Kong, *Powder Technol.*, 2015, **269**, 351–357.
15 F. Ni, J. He, Y. Wang and Z. Luan, *Journal of Water Process Engineering*, 2015, **6**, 158–165.
16 K. L. Scrivener, J.-L. Cabiron and R. Letourneux, *Cem. Concr. Res.*, 1999, **29**, 1215–1223.
17 N. Ukrainczyk and T. Matusinović, *Cem. Concr. Res.*, 2010, **40**, 128–136.
18 V. Antonovič, J. Kerienė, R. Boris and M. Aleknevičius, *Procedia Eng.*, 2013, **57**, 99–106.
19 W. Khaliq and H. A. Khan, *Constr. Build. Mater.*, 2015, **94**, 475–487.
20 N. K. Lee, K. T. Koh, S. H. Park and G. S. Ryu, *Cem. Concr. Res.*, 2017, **102**, 109–118.
21 A. Baradaran-Nasiri and M. Nematzadeh, *Constr. Build. Mater.*, 2017, **147**, 865–875.
22 Y. Su, H. Cui, Q. Li, S. Gao and J. K. Shang, *Water Res.*, 2013, **47**, 5018–5026.
23 J. Lin, Y. Zhan, H. Wang, M. Chu, C. Wang, Y. He and X. Wang, *Chem. Eng. J.*, 2016, **309**, 118–129.
24 D. Xu, J. Lu, S. Yan and R. Xiao, *RSC Adv.*, 2018, **8**, 742–751.
25 H. Hatami, A. Fotovat and A. Halajnia, *Appl. Clay Sci.*, 2018, **152**, 333–341.
26 N. Sleiman, V. Deluchat, M. Wazne, M. Mallet, A. Courtin-Nomade, V. Kazpard and M. Baudu, *Colloids Surf., A*, 2017, **514**, 1–10.
27 D. Mitrogiannis, M. Psychoyou, I. Baziotis, V. J. Inglezakis, N. Koukouzas, N. Tsoukalas, D. Palles, E. Kamitsos, G. Oikonomou and G. Markou, *Chem. Eng. J.*, 2017, **320**, 510–522.
28 Y. Zhao, Q. Yue, Q. Li, X. Xu, Z. Yang, X. Wang, B. Gao and H. Yu, *Chem. Eng. J.*, 2012, **193–194**, 161–168.
29 L. G. Yan, Y. Y. Xu, H. Q. Yu, X. D. Xin, Q. Wei and B. Du, *J. Hazard. Mater.*, 2010, **179**, 244.
30 C. Zhang, Y. Li, F. Wang, Z. Yu, J. Wei, Z. Yang, C. Ma, Z. Li, Z. Y. Xu and G. Zeng, *Appl. Surf. Sci.*, 2017, 396.
31 H. Yin, M. Kong and C. Fan, *Water Res.*, 2013, **47**, 4247–4258.
32 M. El Bouraie and A. A. Masoud, *Appl. Clay Sci.*, 2017, **140**, 157–164.
33 L. G. Yan, K. Yang, R. R. Shan, T. Yan, J. Wei, S. J. Yu, H. Q. Yu and B. Du, *J. Colloid Interface Sci.*, 2015, **448**, 508–516.
34 J. Das, B. S. Patra, N. Baliarsingh and K. M. Parida, *Appl. Clay Sci.*, 2006, **32**, 252–260.
35 X. Yang, D. Wang, Z. Sun and H. Tang, *Colloids Surf., A*, 2007, **297**, 84–90.
36 Y. He, H. Lin, Y. Dong and L. Wang, *Appl. Surf. Sci.*, 2017, 426.
37 W. Y. Huang, R. H. Zhu, F. He, D. Li, Y. Zhu and Y. M. Zhang, *Chem. Eng. J.*, 2013, **228**, 679–687.
38 S. Yang, Y. Zhao, D. Ding, Y. Wang, C. Feng, Z. Lei, Y. Yang and Z. Zhang, *Chem. Eng. J.*, 2013, **220**, 367–374.
39 D. Chen, S. Xie, C. Chen, H. Quan, L. Hua, X. Luo and L. Guo, *RSC Adv.*, 2017, **7**, 54969–54979.
40 M. V. Subbaiah and D. S. Kim, *Ecotoxicol. Environ. Saf.*, 2016, **128**, 109.
41 N. A. Oladoja and B. Helmreich, *Journal of Water Process Engineering*, 2016, **9**, 58–66.

42 N. I. Chubar, V. A. Kanibolotskyy, V. V. Strelko, G. G. Gallios, V. F. Samanidou, T. O. Shaposhnikova, V. G. Milgrandt and I. Z. Zhuravlev, *Colloids Surf., A*, 2005, **255**, 55–63.

43 T.-H. Hsia, S.-L. Lo, C.-F. Lin and D.-Y. Lee, *Colloids Surf., A*, 1994, **85**, 1–7.

44 J. Antelo, M. Avena, S. Fiol, R. López and F. Arce, *J. Colloid Interface Sci.*, 2005, **285**, 476–486.

45 L. Reig, L. Soriano, M. V. Borrachero, J. Monzó and J. Payá, *Cem. Concr. Compos.*, 2016, **65**, 177–185.